33RD INTERNATIONAL COSMIC RAY CONFERENCE, RIO DE JANEIRO 2013
THE ASTROPARTICLE PHYSICS CONFERENCE

ICRC 2013

Tunka-133: Main Experimental Results of 3 Year Operation

V.V. PROSIN[1], FOR THE TUNKA COLLABORATION: S.F. BEREZHNEV[1], N.M. BUDNEV[2], A. CHIAVASSA[5], O.A. CHVALAEV[2], O.A. GRESS[2], A.N. DYACHOK[2], S.N. EPIMAKHOV[7], N.I. KARPOV[1], N.N. KALMYKOV[1], E.N. KONSTANTINOV[2], A.V. KOROBCHENKO[2], E.E. KOROSTELEVA[1], V.A. KOZHIN[1], L.A. KUZMICHEV[1], B.K. LUBSANDORZHIEV[3], N.B. LUBSANDORZHIEV[3], R.R. MIRGAZOV[2], M.I. PANASYUK[1], L.V. PAN'KOV[2], E.G. POPOVA[1], V.S. PTUSKIN[4], YU.A. SEMENEY[2], A.A. SILAEV[1], A.A. SILAEV(JUNIOR)[1], A.V. SKURIKHIN[1], C. SPIERING[6], L.G. SVESHNIKOVA[1], I.V. YASHIN[1], A.V. ZAGORODNIKOV[2].

[1] *Skobeltsyn Institute of Nuclear Physics MSU, Moscow, Russia*
[2] *Institute of Applied Physics ISU, Irkutsk, Russia*
[3] *Institute for Nuclear Research of RAS, Moscow, Russia*
[4] *IZMIRAN, Troitsk, Moscow Region, Russia*
[5] *Dipartimento di Fisica Generale Universiteta di Torino and INFN, Torino, Italy*
[6] *DESY, Zeuthen, Germany*
[7] *Hamburg University, Hamburg, Germany*

v-prosin@yandex.ru

Abstract: We have analyzed data taken over three winter seasons 2009-2012 with the air shower array Tunka-133 and present the results in this paper. We also describe improved methods of EAS parameter reconstruction which are suitable for shower core positions both inside and outside the array. We present the primary CR energy spectrum in the range of 10^{15} - 10^{18} eV. We also discuss the variation of the X_{max} distribution parameters with energy and corresponding variation of the primary mass composition.

Keywords: Tunka-133, spectrum, composition, Cherenkov light.

1 Introduction

The study of primary energy spectrum and mass composition in the energy range of 10^{15} - 10^{18} eV is of crucial importance for understanding origin and propagation of cosmic rays in the Galaxy.

To measure the primary energy spectrum and mass composition of cosmic rays in the mentioned energy range, the new array Tunka-133 ([1], [2]), with nearly 1 km^2 geometrical area has been deployed in the Tunka Valley, Siberia. It records EAS Cherenkov light using the atmosphere of the Earth as a huge calorimeter, resulting in a better energy resolution ($\sim$ 15%) than EAS arrays detecting only charged particles.

The array initially consisted of 133 detectors arranged in 19 compact subarrays (called *clusters* in the following). An essential improvement of the array was made in 2011: the addition of 6 clusters around the basic array, at distances of about 1 km from the center. This extention results in an increase of the effective area for extremely high energies ($> 10^{17}$ eV) by a factor of 3 nearly. The details will be reported in this proceedings [3].

2 EAS parameter reconstruction

The primary data record for each Cherenkov light detector contains 1024 amplitude values in steps of 5 ns [4]. Thus each pulse waveform is recorded over 5 μs. To derive the three main parameters of the pulse: pulse peak amplitude A_i, front delay t_i at a level 0.25 of A_i, and pulse area Q_i, each pulse is fitted with a specially developed smoothing curve [5]. A fourth pulse parameter is the effective width τ_{eff} determined as:

$$\tau_{eff} = Q_i/(1.24 \cdot A_i), \tag{1}$$

The accuracy of this parameter is better than that of the pulse width (FWHM) used earlier. The additional coefficient (1.24) "normalizes" τ_{eff} to FWHM.

The reconstruction of the EAS core position is performed with a new method – fitting measured amplitudes A_i with an amplitude distance function (ADF):

$$A(R) = A(200) \cdot f(R), \tag{2}$$

The function $f(R)$ is a fit to four different parametrizations according to the distance R (in meters) to the shower core:

$$f(R) = \begin{cases} \exp\left(\frac{(R_{\rm kn}-R)}{R_0}\left(1+\frac{3}{R+2}\right)\right), \\ \qquad\qquad R < R_{\rm kn} \\ \left(\frac{200}{R}\right)^{b_2}, \qquad 200\,m \geq R \geq R_{\rm kn} \\ \left(\left(\frac{R}{200}+a\right)/(1+a)\right)^{-b_A}, \\ \qquad\qquad 400{\rm m} \geq R \geq 200{\rm m} \\ \left(\left(\frac{R}{200}+1\right)/2\right)^{-b_A}, \\ \qquad\qquad R > 400\,{\rm m} \end{cases} \tag{3}$$

All four variables in equation (3) (R_0, $R_{\rm kn}$, a and b_2), describing the ADF shape in the different ranges of core distance are related to a single parameter of the ADF shape – the steepness b_A:

$$
\begin{aligned}
&d = b_A - 5, \lg d = \log\ d,\\
&R_0 = 275/d,\\
&R_{\rm kn} = 145 - 115\cdot\lg d,\\
&a = 0.89 - 0.29\cdot\lg d,\\
&b_2 = \begin{cases} 2.4 + 2\cdot(\lg d - 0.15), & b_A \geq 6.41\\ 2.4, & b_A < 6.41 \end{cases}
\end{aligned}
\qquad (4)
$$

As a measure of energy we use the Cherenkov light flux density at a core distance of 200 m - $Q(200)$. The connection between the EAS energy E_0 and $Q(200)$ can be expressed by the following formula:

$$E_0 = C\cdot Q(200)^g \qquad (5)$$

It was found from CORSIKA simulations, that for the energy range of $10^{16} - 10^{18}$ eV, the zenith angle range of $0^\circ - 45^\circ$ and a complex composition, consisting of equal contribution of protons and iron nuclei, the value of the index g is 0.94.

To reconstruct the EAS energy from the Cherenkov light flux one needs to know absolute sensitivities of the Cherenkov detectors and the atmosphere transparency. To avoid these problems, the method of normalization of the integral energy spectrum to a reference spectrum is used. The reference energy spectrum was measured by the QUEST experiment [6]. The integral energy spectrum obtained for each night of the Tunka-133 operation is normalised to that reference spectrum.

3 Experimental data

The Cherenkov light array Tunka-133 operates in clear moonless nights every year since October till the beginning of April. During other seasons nights are too short and weather conditions are mostly unsatisfactory. The data taking by the Tunka-133 array continued during four winter seasons 2009-2010, 2010-2011, 2011-2012 and 2012-2013. The data of the last season are still being analysed. Here we present the data of the first 3 seasons. The total time of data acquisition is 980 hrs. The mean trigger rate was about 2 Hz. The number of recorded events is about $6\cdot10^6$. Such an amount of recorded data provided the possibility of calibration of the apparatus using the data itself.

4 Calibration

The methods of amplitude calibration have been described in [7].

The timing calibration of the detectors inside a single cluster consists of the correction of apparative delays and results in shower fronts which are plane within an accuracy of better than 1 ns.

The obtained calibration corrections are used for preliminary reconstruction of EAS core position.

At the second step of the timing calibration we select large showers with more than 8 hitted clusters and reconstruct the shower front assuming a curved shape as derived from CORSIKA simulations:

$$D = ((200 + R)/R_s)^2 \qquad (6)$$

where D, R and R_s are measured in meters.

The space base of the pulse delay analysis is more than 500 m for such events. So the apparatus error of cluster synchronization (about 10 ns) can lead to the error in the arrival direction less than 0.4°.

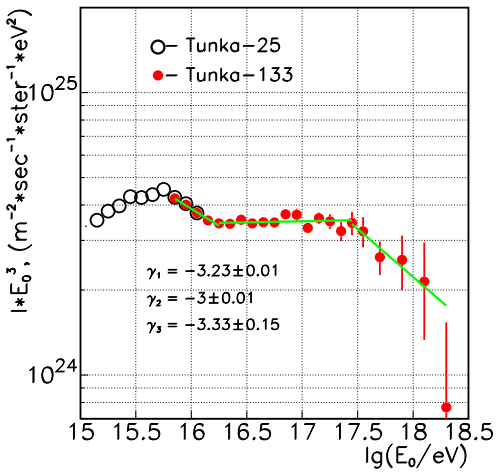

Figure 1: Primary CR energy spectrum

During this step we correct the calibration coefficients a second time so that the EAS axis direction measured by each single cluster coincides with multi-cluster derived axis direction with an accuracy better than 0.5°.

5 Energy spectrum

For the reconstruction of the energy spectrum, events with a core position inside a circle of radius $R = 450$ m from the center of the array were selected. The EAS zenith angle of events used for the spectral measurement was constrained to $< 45^\circ$. With these selections, a 100% registration efficiency is reached for energies larger than $6\cdot10^{15}$ eV. The total statistics above that energy is 170 000 events, 60 000 of them with $E_0 \geq 10^{16}$ eV and 600 with $E_0 \geq 10^{17}$ eV.

We found that also for events with R between 450 m and 800 m, the energy spectrum can be reconstructed. Above some energy threshold ($5\cdot10^{16}$ eV) it is in good agreement with the spectrum for events with $R < 450$ m [4]. Based on these results we reconstruct the combined energy spectrum (Fig.1) for events with $R < 450$ m for $E_0 < 10^{17}$ eV and events with $R < 800$ m for higher energies. The combined spectrum contains about 1900 events with $E_0 > 10^{17}$ eV.

The energy spectrum of Tunka-133 is compared with that of Tunka-25 [6], the predecessor of Tunka-133, in Fig.1. The energy spectrum above the knee looks rather complicated. One can see that the spectrum can be fitted by power laws with 3 different power law indices:
$3.23 \pm (0.01)^{stat} \pm (0.05)^{syst}$ for $6\cdot10^{15} - 2\cdot10^{16}$ eV,
$3.00 \pm (0.01)^{stat} \pm (0.05)^{syst}$ for $2\cdot10^{16} - 3\cdot10^{17}$ eV,
$3.33 \pm (0.15)^{stat} \pm (0.05)^{syst}$ for $3\cdot10^{17} - 10^{18}$ eV.

5.1 Comparison with results of other experiments

A comparison of the Tunka-133 spectrum with the results of other experiments is presented in Fig.2. The energy range covered by our spectrum ($10^{16} - 10^{18}$ eV) is nearly the same as covered by the KASCADE-Grande array data [8].

Both spectra reproduce the same structures: decrease of power law index at $2\cdot10^{16}$ eV and an increase at $3\cdot10^{17}$ eV.

The points of Tunka-133 spectrum coincide with that

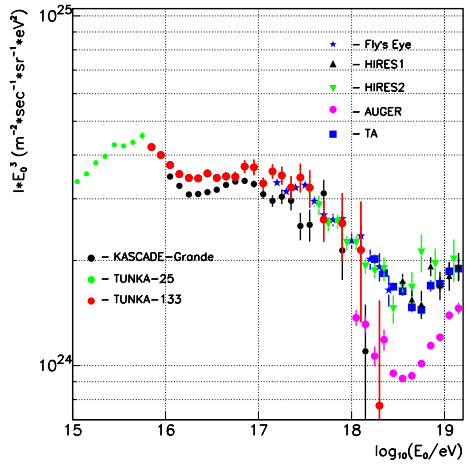

Figure 2: Combined primary energy spectrum: comparison with some other experimental data

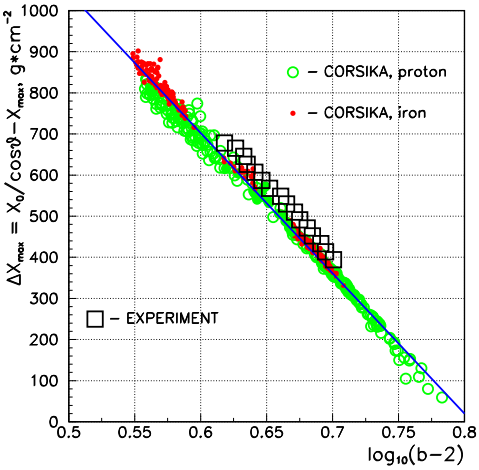

Figure 3: Dependence of the relative EAS maximum position ΔX_{max} on ADF steepness log $b_A - 2)$

of the Fly's Eye and HiRes experiments in the range of $2 \cdot 10^{17} - 10^{18}$ eV. These spectra are consistent with the spectrum of the present TA array at higher energies.

6 Mass composition

To get a uniform estimation for b_A over a wide range of energies, we remove from the analysis detectors at core distances larger than 250 m during the last step of parameter reconstruction.

6.1 Two methods of X_{max} measurement

Recording the pulse waveform for each detector allows to use two methods of X_{max} reconstruction, which were developed for our experiment. The first is based on the shape of the ADF (see above) and called *b*-method. The second method, the τ-method, is based on an analysis of the width of the Cherenkov pulses.

The ADF shape is described by an expression with a single parameter, the steepness b_A (see above). CORSIKA simulation prooves that the steepness b_A is strictly connected with the relative position of the EAS maximum ($\Delta X_{max} = X_0/cos\theta - X_{max}$):

$$\Delta X_{max} = A - B \cdot \log\,(b_A - 2) \qquad (7)$$

MC simulations show, that this relation does not depend on energy, zenith angle of showers, mass composition and the model of nuclear interaction used for the simulation. A plot of 503 simulated events both for protons and iron, for the energy range 10^{16} – 10^{17} eV and zenith angles from 0° to 45° is shown in Fig.3.

The τ-method uses the sensitivity of the pulse width at some fixed core distance to the position of the EAS maximum. We fixed this distance to 400 m and recalculated the values measured with detectors at distances between 200 and 450 m from the core. To recalculate the pulse width to 400 m, the width-distance function (WDF) is used. This function was constructed on the basis of CORSIKA simulation and described in [9]. It was also shown [9], that the value of $\tau(400)$ is connected with the thickness of the atmosphere between the detector and X_{max} ($\Delta X_{max} = X_0/cos\theta - X_{max}$) by the expression:

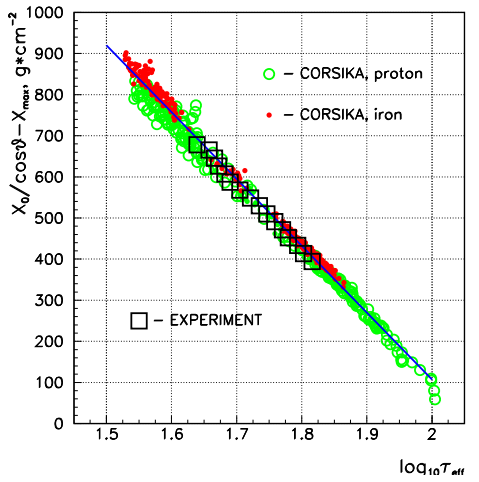

Figure 4: Dependence of the relative EAS maximum position ΔX_{max} on log $(\tau_{eff}(400))$

$$\Delta X_{max} = C - D \cdot \log\ \tau_{eff}(400). \qquad (8)$$

This relation is correct for any primary nucleus, any energy and zenith angle of the shower and any interaction model, as in the case of ADF steepness mentioned above. The plot of the simulated events is shown in Fig.4.

6.2 Phenomenological approach

The phenomenological approach means the experimental check of the correlation between the measured parameter of the shower and the position of the maximum. We start from the parameter $\tau_{eff}(400)$. Its zenith angle dependence ($log\ \tau_{eff}(400)$ vs. $1/cos\theta$) can be easily recalculated to the connection between log $(\tau_{eff}(400))$ and ΔX_{max}. The only value which we need to add to this analysis is the mean $< X_{max} >$ for the energy bin chosen for the analysis. The logaritmic energy bin $16.4 < \log\,(E_0/eV) < 16.5$ is chosen, and it is assumed that $< X_{max} >= 580\,\mathrm{g{\cdot}cm^{-2}}$ for this energy. As a result we get consistency with the CORSIKA simulated correlation as shown in Fig.4. The points are ob-

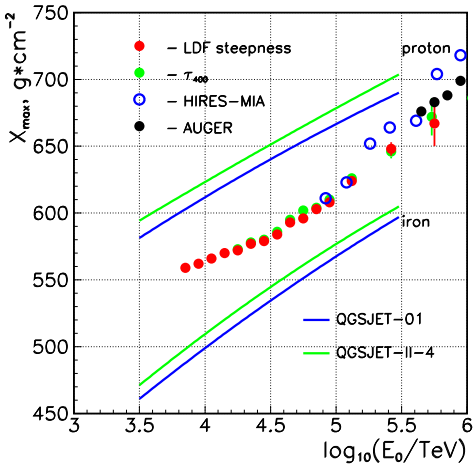

Figure 5: Experimental X_{max} vs. primary energy.

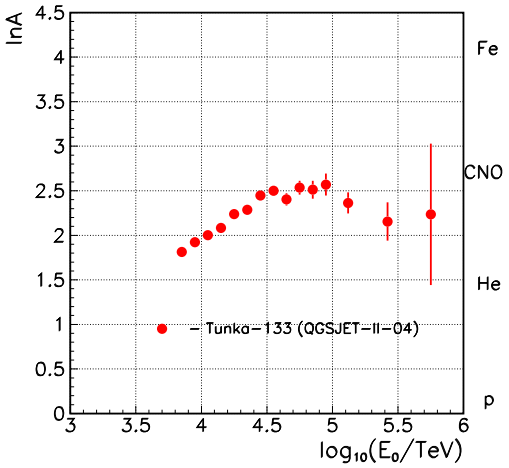

Figure 6: Experimental ln A vs. primary energy.

tained from about 3600 events in this energy bin. The phenomenological values of the constants in the expression (8) are as follows: $C = 3344\,\mathrm{g\cdot cm^{-2}}$, $D = 1624\,\mathrm{g\cdot cm^{-2}}$.

A similar procedure for the same energy has been used for the second parameter b_A. The result is shown in Fig.3. The experimental dependence deviates slightly from the simulated one. This can happen because of the more complicated character of the parameter b_A. The phenomenological points can be fitted with the expression (7) with the values: $A = 2865\,\mathrm{g\cdot cm^{-2}}$, $B = 3519\,\mathrm{g\cdot cm^{-2}}$.

These phenomenological expressions have been used for the measurement of X_{max} for each individual event.

6.3 Estimate of X_{max} experimental error

The use of two independent methods of X_{max} measurement for each individual event allow estimating the experimental error $\sigma_{exp}(X_{max})$ using the experimental data itself. We analyze the distribution of the difference: $\delta X_{max} = X_{max,\tau} - X_{max,b}$ – for each energy bin. The RMS of the δX_{max} distribution changes slightly from $48\,\mathrm{g\cdot cm^{-2}}$ at $E_0 = 10^{16}\,\mathrm{eV}$ to $40\pm1\,\mathrm{g\cdot cm^{-2}}$ for energies $E_0 \geq 3\cdot10^{16}\,\mathrm{eV}$. Assuming equal experimental errors for any of the methods we can estimate $\sigma_{exp}(X_{max}) = \delta X_{max}/\sqrt{2}$. So $\sigma_{exp} = 28\pm1\,\mathrm{g\cdot cm^{-2}}$ for $E_0 \geq 3\cdot10^{16}\,\mathrm{eV}$. This value is used in [10] for the analysis of experimental X_{max} distributions.

6.4 X_{max} vs. E_0

The experimental dependence of mean $< X_{max} >$ vs. primary energy E_0 in the energy range of $6\cdot10^{15} - 5\cdot10^{17}\,\mathrm{eV}$ obtained with the two methods described above is presented in Fig.5. Only events where the difference between the two X_{max} values is less than $3\delta X_{max}$ where used. The new measurements are compared with the theoretical curves simulated with old QGSJET-01 and the very new QGSJET-II-04 model for primary protons and iron nuclei. It is seen from Fig.5 that the new model provides a depth of the EAS maximum about $10\,\mathrm{g\cdot cm^{-2}}$ higher than the old one.

The mean values of $< X_{max} >$ can be recalculated to the mean values of $< ln\,A >$ by a simple method of interpolation. The result of such an approach for the points derived from the ADF steepness analysis are shown in Fig.6.

A more complicated analysis of total X_{max} distributions will be presented in [10].

7 Conclusions

1. The primary spectrum above the knee cannot be fitted with a single power law index but with three indices:
$3.23\pm(0.01)^{stat}\pm(0.05)^{syst}$ for $6\cdot10^{15} - 2\cdot10^{16}\,\mathrm{eV}$,
$3.00\pm(0.01)^{stat}\pm(0.05)^{syst}$ for $2\cdot10^{16} - 3\cdot10^{17}\,\mathrm{eV}$,
$3.33\pm(0.15)^{stat}\pm(0.05)^{syst}$ for $3\cdot10^{17} - 10^{18}\,\mathrm{eV}$.

2. The high energy tail of the spectrum is compatible with the Fly's Eye, HiRes and TA spectra.

3. The X_{max} values are compatible with that of HiRes and Auger.

4. The mass composition changes to a heavier composition in the energy range $10^{16} - 3\cdot10^{16}$ eV, stays heavy till 10^{17} eV and starts changing to a lighter composition from about 10^{17} eV.

Acknowledgment: This work was supported by the Russian Federation Ministry of Science and Education (G/C 14.518.11.7046), the Russian Foundation for Basic Research (Grants 11-02-00409, 13-02-00214, 13-02-12095)

References

[1] N.M.Budnev et al. (Tunka Collaboration), Proc. 30th ICRC, Merida, Yucatan,Mexico, 2007, arXiv: 0801.3037.
[2] N.M.Budnev et al. (Tunka Collaboration), Proc. 31th ICRC, Lodz, Poland, 1 (2009) 1069. arXiv: 1003.0089.
[3] N.M.Budnev et al. (Tunka Collaboration), This Conference, ID=0418.
[4] S.F. Berezhnev et al. (Tunka Collaboration), NIM A 692 (2012) 98-105.
[5] E.E.Korosteleva et al. Proc. 31th ICRC, Lodz, Poland, 1 (2009) 0492.
[6] E.E. Korosteleva et al., Nuclear Physics B (Proc. Supp.), 2007 **165**: 74-80
[7] N.M. Budnev et al. (Tunka Collaboration), Proc. 29th ICRC, Pune, India, 2005 **6**: 257-260
[8] A. Haungs for KASCADE-Grande collaboration, Proc. of 32th ICRC, Beijing 2011, ID=677
[9] B.V. Antokhonov et al. (Tunka Collaboration), Nuclear Physics B (Proc. Supp.), 2011 **212-213**: 53-58
[10] S.N.Epimakhov et al. (Tunka Collaboration), This Conference, ID=0326.